A Self-Consistent Field Analysis of the Neurofilament Brush with Amino-Acid Resolution

E. B. Zhulina* and F. A. M. Leermakers†
*Institute of Macromolecular Compounds, Russian Academy of Sciences, St. Petersburg, Russia; and †Laboratory of Physical Chemistry and Colloid Science, Wageningen University, Wageningen, The Netherlands

ABSTRACT Using the numerical model of Scheutjens and Fleer we investigated, on a self-consistent field level, the equilibrium structure of the neurofilament brush formed by the projection domains of NF-H, NF-M, and NF-L proteins. Although the actual amino-acid sequences in the projection domains are coarse-grained, the different (realistic) solubilities of amino-acid residues and the specific distribution of its intrinsic charges inside the arms of the NF proteins are taken explicitly into account. We collect strong evidence that the electrostatic interactions are a dominant force that controls the NF brush structure. There exists a remarkable spatial separation of the H, M, and L tails. In a dephosphorylated NF we found confined and flowerlike conformations for the H and M projection domains, respectively. We demonstrate that the ionization of KSP repeats in NF proteins triggers a conformational transition in the H tail that leads to the expulsion of its terminal (KEP) domain to the periphery of the NF brush. We argue that the phosphorylation of the NF proteins in axons can both increase the interfilament distance and stabilize cross bridges between neurofilaments.

INTRODUCTION

Recent research in neuron physiology shows a large effort to relate the ultrastructure and spatial distribution of intermediate filaments in axons and dendrites to human neurodegenerative diseases. Abnormal accumulation and aggregation of neurofilaments (NFs) is linked to the development of such diseases as amyotrophic lateral sclerosis, Lewy-body-type dementia, and Parkinson disease (1). Neurofilaments are almost exclusively expressed in neuronal cells. Together with other intermediate filaments they give rise to a cellular cytoskeleton, a scaffold that ensures various processes in neurites. Although the necessity of NFs is not proved for nervous system development, it is generally recognized that NFs are involved in the control of the radial growth of large myelinated axons and the maintenance of the axonal caliber (1,2).

It is well documented that NFs are composed of three subunit proteins labeled as NF-L (light), NF-M (medium), and NF-H (heavy) according to their molecular weights (3). All of them contain a rigid domain of ~310 amino-acid (aa) residues close to the N-terminus and a so-called projection domain (nonstructured flexible tail) at the C-terminus. In a human NF the numbers of aa residues are $N_H = 607$, $N_M = 504$, and $N_L = 142$ in the NF-H, NF-M, and NF-L projection domains, respectively. These numbers slightly vary in different species: rodents, mammals, etc.

NF proteins self-assemble to form neurofilaments. This process occurs through a series of steps that involve the initial formation of L-L, L-M, and L-H coiled-coil dimers, and the subsequent association of dimers in tetramers, protofibrils, and protofilaments (3). In a mature NF, the backbone consists of four protofilaments (4), and its radius R is ~5 nm. In human adult NF, the stoichiometry of H/M/L proteins is 2:3:7 (3). The projection domains are separated along the NF backbone (5). The backbone comprises 16 dimers in its cross section (4), and therefore one finds ~18 L tails, 8 M tails, and 5 H tails per backbone segment of length 45–47 nm (the size of the rigid domains of the NF proteins). These numbers are consistent with an average distance of 3–4 nm between long tails reported in earlier studies (6).

The L, M, and H projection domains differ not only in the number of aa residues, but also in their charge distributions. In a dephosphorylated neurofilament, both L and M tails carry an excessive negative charge (mostly due to Glu (E) residues), whereas in the H tail the number of positively and negatively charged residues is almost equal (145 negative and 144 positive charges). Even though the H tail carries just one excess charge and thus constitutes an almost net neutral polyampholyte, electrostatics is important as the gradient in the charge distribution along the chain causes a positively charged peripheral part of the H tail and a negatively charged part near the rigid domain. In the presence of accessory proteins, the terminal part of the H tail (comprising ~190 aa residues) can form a complex with a similar part of some other H tail. On the basis of this unique feature of the H projection domains, the so-called cross-bridge model was formulated approximately 20 years ago. The cross-bridge model specifies the structural organization of the NF cytoskeleton (7). In the framework of this model, the cross bridges between H tails of neighboring NFs keep the neurofilamental network intact and, thereby, determine the interfilament distance. Accordingly, the NF-H proteins are

Submitted September 15, 2006, and accepted for publication January 3, 2007.

Address reprint requests to F. Leermakers, Tel.: 31-317-482268; E-mail: frans.leermakers@wur.nl.

Editor: Ivet Bahar.

0006-3495/07/09/1421/10 $2.00

doi: 10.1529/biophysj.106.095323

believed to play a major role in controlling the axonal caliber (1).

Gene knockout studies have, however, demonstrated that NF-H null mice exhibit only a slight reduction in the caliber of myelinated axons from the ventral roots (8,9). The targeted disruption of the NF-M protein has more severe effect on the axonal growth, and can result in a significant reduction in NF content and axon atrophy (10). The absence of both NF-H and NF-M proteins provokes alterations in the organization of the neuronal cytoskeleton. A noticeable increase in the microtubule content in large ventral root axons has been reported in double mutant NF-H;NF-M mice (8,10). Mice with a disrupted NF-L gene exhibited severe axonal hypotrophy (11). Because the NF-L protein serves as a partner in the coassembly of L-M and L-H dimers, a lack of this protein leads to an abnormal increase in NF-M and NF-H levels in the cell and can provoke a gradual blockage of axonal transport. An elevation in the NF-L level and the corresponding increase in the NF-L/NF-H and NF-L/NF-M ratios restores the radial growth of axons in transgenic mice. However, the overexpression of human NF-L in transgenic mice was reported to cause severe loss of neurons with age (12).

The transgenic mouse studies (8–12) as well as other lines of evidence (1,13) indicate that the respective roles and the distinct functions of the three neurofilament proteins are not fully comprehended. A theoretical investigation of the neurofilament structure and its properties may therefore provide additional insights into how NFs are involved in the control of the axonal caliber and, thereby, the conductivity of large myelinated axons.

Recently, a novel (polymer brush) model of the neuronal cytoskeleton was formulated (6,13). This model is corroborated by the existing biochemical, biophysical, genetic, and cell biological data, and it promises a mechanism for the mechanical protection of axons and dendrites. Within this framework, the projection domains (side arms) of neurofilaments are envisioned as polymer brushes that mediate the interfilament distances in large axons (Fig. 1). The compression of such polymer brushes gives rise to a repulsive force that prevents the mutual approach of NFs at small distances. This mechanism is similar to the well-known mechanism of steric stabilization of colloid dispersions by polymers (14,15). Together with cross bridges that keep the NF network intact, the nonspecific repulsion between projection domains controls the interfilament distance. A recent study (6) has demonstrated that the liquidlike distribution of interfilament distances in mouse sciatic nerves can be reproduced in Monte Carlo simulations with interfilament interaction potentials derived from the brush theory. In this simulation, the projection domains were modeled as homopolymer chains with a smeared charge distribution. The effect of phosphorylation was incorporated by changing the average degree of ionization of the tails. The model predicted a noticeable increase in the interfilament distance with phosphorylation, whereas the effect of cross-bridging was less significant (6).

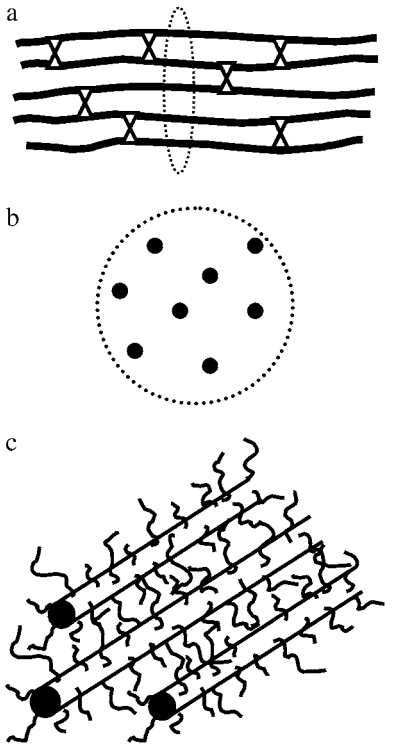

FIGURE 1 Schematic drawing of (*a*) the cytoskeleton with neurofilaments shown by lines and cross bridges indicated by crosses, (*b*) part of the axon cross section with a liquidlike distribution of NFs shown by solid dots, (*c*) NF brushes of projection domains.

From a polymeric point of view the projection domains of a neurofilament, as modeled in this article, constitute a more complex object than biological brushlike structures examined in earlier studies (6,16–18). The NF brush is a cylindrical brush with a radius of the backbone much smaller than the interfilament distance (brush thickness). Tails with three different lengths, $N_H = 607$, $N_M = 504$, and $N_L = 142$, are tethered to the backbone with the stoichiometric ratio H/M/L = 2:3:7. The charge distributions on the tails differ for each protein. Whereas the dephosphorylated H tail is almost a net neutral polyampholyte with total (almost) zero charge, both M and L tails can be envisioned as negatively charged polyelectrolytes. Enzymatic phosphorylation of the H tail occurs mostly through the Arg-Ser-Pro (KSP) repeats, which are located in the central part of the H projection domain (3). The intrinsic structure of such a brush could be quite sensitive to the details of the charge distribution mediated by the phosphorylation of the H and M tails.

The goal of this article is to explore theoretically the equilibrium structure of an individual neurofilament brush and its response to enzymatic phosphorylation of the H and M projection domains. We employ the self-consistent field (SCF) method of Scheutjens and Fleer (19) to numerically model such a system. The Scheutjens-Fleer (SF) method is

widely used in physical chemistry and colloid science to study the behavior of charged and neutral polymers at interfaces, self-assembly of polymers and lipids in solutions, complexation of polymers with surfactants and membranes, etc. (20–23) To the best of our knowledge, this is the first application of the SF model to investigate theoretically the equilibrium internal structure of the neurofilament brush. In Methodology, we describe the model of the NF brush and our simulation technique in more detail and then present Results and Discussion. The summary of our study is presented in Conclusions.

METHODOLOGY

Model

The application of the Scheutjens-Fleer (SF) technique requires coarse-graining of the NF tails. Each aa residue is modeled as a cube with bond length a. The value of a can be estimated from the x-ray crystallography data for aa monomers (www.reciprocalnet.org). The relationship between the density ρ, the molecular weight (MW), and the volume a^3 for a monomer, $a^3 = MW/\rho$, suggests a size $a = 5$–6 Å for the majority of the aa residues. The value of $a = 6$ Å, for the typical size of an aa residue in the glycomacropeptide tail of κ-casein, was used recently to rationalize the dynamic light scattering data in solutions of casein micelles (18). The reported value of the Stokes radius for the polyampholytic H tail, $R_h = 60$ Å (6), is also consistent with the value of $a = 6$ Å. We therefore choose $a = 6$ Å in all our SCF calculations. Note that in the framework of the SF model, solvent (water) molecules as well as salt ions are assumed to have the same (lattice) size a.

The analysis of aa sequences in tails L, M, and H (Human Intermediate Filament Database, http://www.interfil.org/proteins.php) indicates that, under physiological pH ≈ 7 (almost all acidic and basic aa residues are ionized), the electrostatics is expected to be a major factor that determines the NF brush structure. To check this hypothesis, we introduced two different models for the dephosphorylated NF tails.

In the first, simplified model c, the H tail is modeled as an anionic/cationic block copolymer. The M tail is envisioned as an anionic homopolymer, whereas the L tail is modeled as a neutral/anionic block copolymer. The number of aa residues in each of the blocks, and the effective charge per monomer, are indicated in Fig. 2. The solubility parameters of all aa residues are assumed to be the same: the Flory interaction parameter that determines the free energy difference between monomer-water and monomer-monomer and water-water contacts, is $\chi = 0.6$ (this parameter is, by definition, made dimensionless by the thermal energy k_BT). This value of χ corresponds to moderately poor solvent conditions for the aa residues (monomers are weakly attracted to each other). All other interaction parameters for the aa-backbone, aa-ion, ion-ion interactions, etc., are assumed to be zero. This model is referred to as model c to emphasize the copolymer type of coarse-graining of the NF side arms.

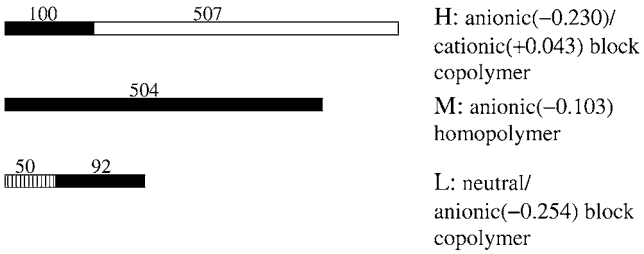

FIGURE 2 Coarse-grained NF-L, NF-M, and NF-H projection domains in model c. Numbers in brackets indicate the partial charge per monomer.

In the second, more refined model, the specific aa sequence and the actual distribution of the charges along each tail are conserved to a larger extent. The set of aa residues is divided into five groups labeled as **A**, **N**, **P**, **M**, and **C**. The apolar aa residues {G, P, C, M, A, L, V, I} constitute group **A**. These monomers have the worst solubility in water and strongly tend to aggregate (their poor solubility is accounted through a large value of the Flory interaction parameter $\chi = 2$). The polar aa residues {Y, Q, H, F, W} that have a better solubility in water ($\chi = 0.6$) constitute group **N**. Acidic aa residues {E, D} that can carry a negative charge belong to group **M**. They are assumed to have a unified value of $pK_a = 5$. Amino-acid residues that can obtain a positive charge, i.e., basic aa residues {K, R}, belong to group **P** and are given a unified value of $pK_b = 5$. Amino-acid residues in both groups **M** and **P** are assumed to have an athermal mixing with water, which is $\chi = 0$. Finally, serine {S}, which is involved in the phosphorylation process and in particular the serine in the KSP repeats, is the only residue in group **C**. Its solubility in water is assumed to be the same as for aa residues in group **N** ($\chi = 0.6$). Note that although threonine {T} and serine {S′} not incorporated in the KSP repeats can also participate in the phosphorylation, we currently keep these {T, S′} residues in group **N**. We therefore restrict our analysis to moderate levels of phosphorylation, i.e., through the ionization of KSP repeats only. (Hyperphosphorylation involving S and T elsewhere in the tails will be considered separately.) We refer to this second model as model f, emphasizing the fine coarse-graining of the NF tails.

Table 1 presents the coarse-grained aa sequences of the H, M, and L projection domains in model f. The digit to the right of each group label (**A**, **N**, **P**, **M**, or **C**) indicates the number of repeating monomers of the specified type (and the brackets are used when there is a sequence of repeating aa residues). The terminal 191 residues in the H tail (shown in *italics* in Table 1) constitute the so-called KEP segment of the H projection domain that participates in cross-bridge formation (3). Interestingly, all the KSP repeats (comprising serine as C monomer in Table 1) are located rather regularly in the central part of the H tail, and the moderate phosphorylation does not perturb the terminal cross-bridge portion of the H projection domain. Similar coarse-graining was performed for the M and L tails (Table 1). Coarse-grained H, M, and L tails were irreversibly tethered to the cylindrical backbone of the NF with appropriate stoichiometry (2:3:7), and the value of $R = 8a$ (corresponding approximately to $R = 5$ nm) for the core radius was used in all the calculations.

METHOD

The numeric SCF method of Scheutjens and Fleer is described in detail in a number of publications (see (19) and references therein). Here, we review only the basic features of this technique.

The ultimate goal of the SCF calculation is to find the equilibrium distance-dependent distributions of all the components in the system, including the monomers of the H, M, and L tails, water, added ions, etc., collected in the volume fraction φ-profiles. In this article, we use the one-dimensional version of the SF model. In the framework of this one-dimensional model, the distributions of all the components depend only on one coordinate z, i.e., the distance from the backbone of the neurofilament, and the target is to find $\varphi_X(z)$ for all species X. Physically the volume fraction $\varphi_X(z)$ is the dimensionless concentration of component X in layer z and it is computed by taking the ratio between the number $n_X(z)$ of segments of type X in layer z and the number of available sites $L(z)$ in layer z, i.e., $\varphi_X(z) = n_X(z)/L(z)$. In the lateral dimension (along the backbone), the distribution of all the components is thus smeared (mean-field approximation). The search for the equilibrium distribution of the components implies introduction of the effective potential fields $u_X(z)$ (for each monomer type X in the system). Each potential u_X acts on its own species X in the system. Through the interaction of each component with its potential field, the current distribution of all the species is determined. In turn, the current distribution $\phi_X(z)$ of the polymer and all ions specifies the potentials acting

TABLE 1 Coarse-grained projection domains in model *f*

The H-chain:

$NA_4N_2A_2$ MA_3PA_2 $NAN_3(AP)_2N$ $M_2(PA)_2AM$ PNMP $MNA_3(M_2N_2)_2$ $(ANM_2)_2M_2PM$ $(APM_3)_2A_2M_4A$ MA_2M_3N PCA_3M_2 A_2NAM PMAP CA_2PM_2 $APCA_2$ MAPC $AMPM_2$ $APCA_2$ MAPC AMPA PCA_2P M_2APC A_2MAP CAMP M_2APC A_2MAP CAMP $APCA_2$ PM_2AP CA_2MA PCAM PAPC A_2PM_2A PCA_2M $APCA_2$ PM_2AP CA_2MA PCAM PAPC $ANPM_2$ APCA MPAP CAMP M_2APC AMPA PCA_2P AMAP CAMP $APCA_2$ PAMA PCAM PAPC A_2PM_2A PCAM PAPC A_2PM_2A PCAM PAPC A_2PM_2A PNAM PAPC A_2PM_2A $P(CAMPAP)_2NA$ MAPC AMAP NA_2PM_2 $APNA_2$ MPNA MPA PCA_2P M_2APC AMPA PCA_2P M_2APA_2 $MPMA_2$ P_2M_2AP CA_2PM_3PA-*$NM(AP)_2MA_2$ P_2AM_3P A_3NAP NM_2P_2M $NP_2M_2A_2$ $P_2MA_2(PA)_2$ $M_2P_2MA_3$ MPAP MNPA MAP_2M_2 $AM_2P_3A_2$ NAMP MA_3PA $MAPM_2$ $(AP)_2MPN$ MA_2P_2M $AM_2(AP)_2M$ $ANPA_2M$ P_2MA_3M P_2MNP M_2PAP_2 AM_2PA $PNM(AP)_2$ M_3PNA NPMA $N(PA)_2MP$ $AMPN_4(MNP)_2$ A_2MPA NM_2PA $(AP)_2$*

The M-chain:

$N_3A_2(NA)_2A_2$ N_3PA_3N AN_2PA NPNP $AMA_2(PA)_2$ N_2PNA $M_2A_2M_2N$ PAM_3P $NMAM_2$ $(A_2N)_2M_2A_3N$ APM_2P_2 MA_2M_2P $M_3(AM)_2M_3A_3$ P_2CA_2P ANA_2MA PM_3AM PM_4AN M_8A_2P NMNA M_2A_2NM $PMAN_2$ MPM_2A MNM_2A $MNM(AM)_3$ $(MA)_2PM_2P_2$ AM_2PN M_2A_2NP M_2A_3MA PAMP AMPA PCA_3P CA_2M_2P $APCA_3$ PCA_2M_2 PAPC A_3PCA_2 M_2PAP CA_3PC A_2M_2PA PCA_2N PCA_2M_2 PAPC A_3PCA_2 M_2APN $PAMA_2$ PAMN PM_3PM $APMA_2$ PM_2PA MP_2M_2P $APMA_2$ MP_3AM NA_2PM_2 A_3MA_2N ANPN APAN AMPM NPM_2A $PA_2N_2(MP)_3$ A_3MA_2N M_3ANM PA_2PA $NP_2M_2A_3$ $N(AM)_2AP$ $M_2A(MN)_2P$ MPAN APM_3P $A_3N_2A_2M$ ANA_2M_2 P_2A_2MP NM_2PA_3 NPNA $MPAN_2$ $(MA_2)_2(NPNA)_2NA$ $N_2PA(M_2N)_2$ NM_2PA_2 N_2P_2AM PAN_3A_3 $PMAN_3M$

The L-chain:

$N_3A_2(NAN)_2N_4$ $(NA)_2P(NA)_2A_2$ $N_5A_2N_2P$ N_2AN_6 A NM_2N_2M AM_2NA MANP AM_2AP $M_2A_2N(MA)_2$ $M_4(PM)_2M(AM_4A)_2M_4A$ PM_2NM_2 APM_4A_2 $M(AM_2)_2NP$ MAM_4P_2 AMA_3M_2 NA_2P_3M

A number behind the segment name (or sequence) indicates the length of this repeat. The following amino-acid assignments were made: $\mathbf{A} \in \{G, P, C, M, A, L, V, I\}$, $\mathbf{N} \in \{Y,Q, H, F, W T, S\}$, $\mathbf{P} \in \{K, R\}$, $\mathbf{M} \in \{E, D\}$, $\mathbf{C} \in \{S\}_{KSP}$. The terminal KEP-segment of the H chain is in italics.

on all the components. The numerical procedure that solves the equations is finished when the potential fields become self-consistent, i.e., the potentials both follow from and determine the volume fraction profiles and—the other way around—the volume fraction profiles both determine and follow from the potentials.

Inherent in the SCF approach, one accounts for the inter- and intrachain excluded-volume interactions through the self-consistent potentials. A rigorous account for interchain excluded-volume interactions requires the analysis of all statistical weights of self-avoiding chains. Such a job requires excessive computational costs. For polymer brushes, whose chains are strongly stretched beyond the Gaussian dimensions (due to the local high osmotic pressure), it is a conventional approximation to use the more primitive freely-jointed chain model. Within this model there exists an efficient propagator scheme to add up all the statistical weights of all possible and allowed conformations of the polymer molecules in the self-consistent potential fields. We refer to the literature for this propagator formalism (19).

As mentioned above, the NF system is expected to be significantly affected by the electrostatic interactions. Within the SCF approach it is therefore essential to specify the electrostatic potential. The Poisson equation for a cylindrical coordinate system accounting for local gradients in dielectric permittivity,

$$\frac{1}{z}\frac{\partial}{\partial z}\left[\epsilon(z) z \frac{\partial \psi}{\partial z}\right] = -\rho(z), \tag{1}$$

is solved rigorously with the accuracy of the lattice-type discretization. To do so the local dielectric permittivity is evaluated by the volume fraction average $\epsilon(z) = \epsilon_0 \sum_X \varphi_X(z)\epsilon_X$, where ϵ_X is the relative dielectric permittivity of a pure phase composed of species of type X. In our calculations we take $\epsilon_A = \epsilon_{backbone} = 2$, for all charged species $X = Na, Cl, M, P$ we have $\epsilon_X = 5$, and all other components have a relative dielectric constant of 80. (Here, *Na* and *Cl* are sodium and chloride ions due to added salt.) The dielectric permittivity of vacuum is given by ϵ_0. The spatial charge distribution follows from the volume fraction profiles for all the components (amino-acid residues, salt ions, and water). Some of the species in the system can be either in a neutral state or in a charged one (depending on pH, local electrostatic potential, etc.). Let k be a variable pointing to an internal state of such species, and $\alpha_{X,k}$ be the fraction of segments of type X in internal state k. When the valency of this state is given by $\nu_{X,k}$, the charge density distribution is given by

$$\rho(z) = e\sum_X \sum_k \varphi_X(z)\alpha_{X,i}(z)\nu_{X,k}, \tag{2}$$

where e is the elementary charge. It is seen from Eq. 2 that the local degree of dissociation of the weak amino-acid residues (and of water) is accounted for. Details may be found elsewhere (24).

RESULTS AND DISCUSSION

Individual dephosphorylated NF

We start with the structural organization of the projection domains in an individual dephosphorylated NF. Properties of such filaments in vitro are experimentally probed in an environment that is generally different from that inside the axon. In this study we fix pH = 7 (i.e., close to the physiological value) and the solution salinity 0.01 M of 1:1 salt. Although this ionic strength is lower than in the living cells ($\simeq$0.15 M), we choose this value in the SCF calculation to emphasize the structural changes in an individual NF brush induced by the phosphorylation of the projection domains. A comprehensive analysis of the effect of the salinity on the structure of NFs will be presented in our forthcoming work.

Fig. 3, *a* and *b*, demonstrates the polymer density profiles (volume fractions) $\varphi(z)$ for the H, M, and L projection domains in an isolated dephosphorylated NF, as a function of the distance z in both models *c* and *f*. These profiles are obtained by summation of the volume fractions $\varphi_X(z)$ for all species $X = \mathbf{A}, \mathbf{N}, \mathbf{P}, \mathbf{M}, \mathbf{C}$ that belong to a given tail (H, M, or L). The distance from the backbone is measured in units of the monomer size a. That is, the absolute value of the distance from the backbone of NF is az where $a = 6$ Å.

Fig. 4 shows the volume fraction of the end monomers, $g(z)$, for the H, M, and L tails in both models *f* (*solid lines*) and *c* (*dashed lines*).

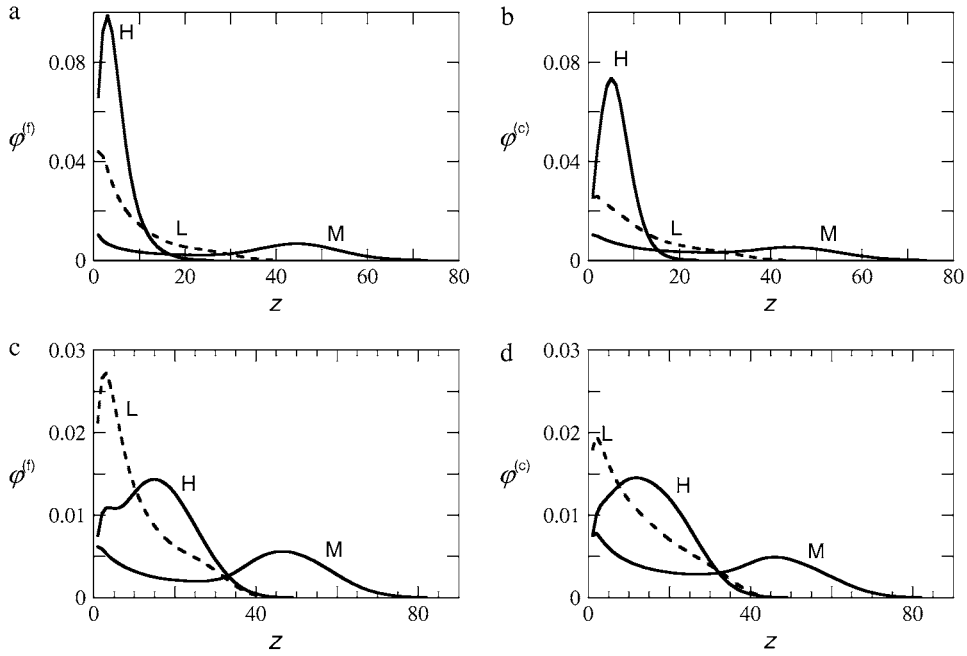

FIGURE 3 Polymer volume fraction profiles in NF brush with hydrophobic (*a*,*b*) and without hydrophobic interactions (*c*,*d*). The fine model (*a*,*c*) and the coarse model (*b*,*d*). Results for the *L* projection domains are given by dashed lines, predictions for the other two are given by solid lines. pH = 7 and the ionic strength $c_s = 1 \times 10^{-2}$ M. Other parameters are given in the text.

Fig. 5, *a* and *b*, presents the electrostatic potential profile $\psi(z)$ in an individual isolated NF (in Volts) and the volume fraction of charges $q(z)/e$ (including the charges due to the salt ions) as a function of the distance z from the backbone (*solid lines* for the fine model *f* and *dashed lines* for the coarse model *c*).

Several distinctive features of the NF brush organization are seen from these plots.

1. The protein (polymer) density profiles (Fig. 3, *a* and *b*), the distribution of end monomers (Fig. 4) and the NF electrostatic potential (Fig. 5) are surprisingly similar in the two models, *c* and *f*. This similarity confirms the initial expectation that the electrostatics would be a dominant factor to determine the conformations of the H, M, and L tails in the NF brush. The basic features of the charge distribution on the tails are captured already in the simple model *c*. Small differences in the absolute values of the polymer volume fractions for the H and L tails are found mostly near the backbone. Smaller values of $\varphi_H(z)$ in model *c* are attributed to a better average solubility of the monomers ($\chi = 0.6$ for all aa residues). Recall that, in model *f*, the apolar aa residues (comprising group A) exhibit an inferior solubility in water, and the total number of such monomers in the H tail is noticeable near the backbone of neurofilament. The predominance of the electrostatic forces does not imply that the effect of hydrophobic interactions can fully be neglected. To demonstrate the contribution of nonelectrostatic (hydrophobic) interactions, Fig. 3, *c* and *d*, presents polymer density profiles $\varphi(z)$ for a hypothetical case when all the unfavorable aa-water interactions are switched off ($\chi = 0$). Comparison of the polymer distributions of Fig. 3, *a* and *b*, and Fig. 3, *c* and *d*, indicates that whereas the structure of the peripheral parts of NF brush is retained, the shapes of density profiles $\varphi_H(z)$ and $\varphi_L(z)$ change rather noticeably. When the nonelectrostatic interactions are turned off, the smallest chains are found near the backbone, whereas the longest ones are in the proximal part of the brush. This is reversed when the interactions are taken realistically. Therefore, both types of interactions (electrostatic and nonelectrostatic) are essential to establish the equilibrium structure of a neurofilament brush.
2. The polymer density profiles $\varphi(z)$ in Fig. 3, *a* and *b*, and the distribution functions of the end monomers $g(z)$ in Fig. 4, demonstrate the striking spatial separation of the

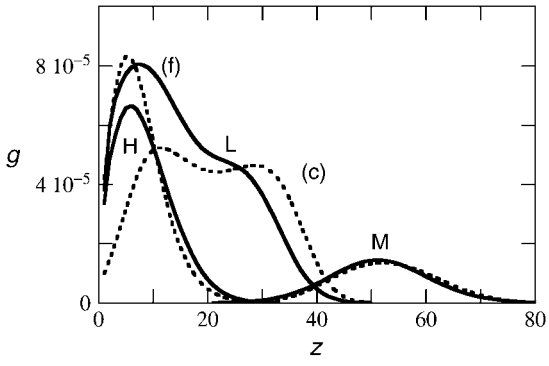

FIGURE 4 The volume fraction profiles of the end monomers $g(z)$ for the H, M, and L tails in model *f* (*solid lines*) and model *c* (*dashed lines*), corresponding to the results of Fig. 3, *a* and *b* (with hydrophobic interactions).

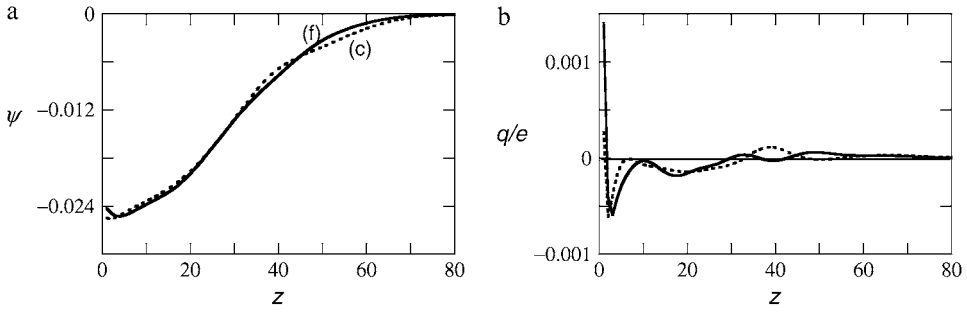

FIGURE 5 The electrostatic potential $\psi(z)$ (*a*) in Volts, and the dimensionless overall charge distribution $q(z)/e$ (*b*) as a function of the distance z from the backbone of the NF.

tails in a dephosphorylated NF. The largest tails (H) are localized in the presurface layer near the backbone of the NF, the tails with intermediate length (M) are expelled to the periphery of the brush, whereas the shortest tails (L) protrude outside of the presurface layer and fill the proximal region of the brush. Such organization of the NF brush seems surprising only at the first glance. The presence of numerous L tails (that overcompensate by far the positive charge on distal parts of the H tails) leads to the appearance of a negatively charged zone near the NF backbone. The longest tails (H) are embedded totally into this zone, whereas the negatively charged M tails are expelled outside to the periphery of the brush. The distribution of end monomers in Fig. 4 confirms this picture. The end points of the M tails are found only at the periphery of the brush, whereas the end points of the H tails are localized near the backbone. Interestingly, the end points for the L tails exhibit a bimodal distribution that is less pronounced in the more accurate model *f*.

3. Fig. 5, *a* and *b*, demonstrates that the electrostatic interactions inside an isolated individual NF immersed in an electrolyte solution of 0.01 M of a 1:1 salt are essentially screened, and the concentration of the overall charge $q(z)$ is close to zero almost everywhere in the brush. The maximal value of electrostatic potential $\psi(z)$ near the backbone, $z = 0$, is ~25 mV. Interestingly, the edges of the three different sublayers containing H, L, and M side arms in a neurofilament brush are accompanied by three ''electric double-layers'' (extrema in concentration of the total charge $q(z)$ in Fig. 5 *b*). Here the deviations in $q(z)$ from zero are most noticeable.
4. The analysis of the polymer density decay for the M tails indicates that, in the proximal region of the brush $\varphi_M(z) \sim (R/a+z)^{-\beta_M}$, where the exponent β_M is close to unity. The total number of monomers $n_M(z)$ per unit length a of the NF can be obtained by the summation of the polymer volume fraction $\varphi_M(z)$ in the cylindrical layer at a distance z from the backbone (Fig. 6). Because the total number of sites $L(z)$ in a cylindrical layer increases as $L(z) \sim (R/a + z)$, the number of monomers is $n_M(z) \sim \varphi_M(z) L(z) \sim (R/a+z)^{1-\beta_M}$. The value of $\beta_M = 1$ for the M tails implies that $n_M(z)$ is independent of the distance z. Fig. 6 clearly indicates that, in the proximal region of the NF brush, $n_M(z) \approx 0.45$ is virtually independent of z. Because the free ends of the M tails are localized at the periphery of the NF brush (Fig. 4, portions of the M tails in the proximal region of the NF brush are stretched almost uniformly. Taking into account the linear grafting density of the M tails (~1 M-tail per 5.5 nm $\approx 9a$ along the backbone counter) we find that each M tail contributes ~4 aa residues per unit distance a in the radial direction. Therefore, the M tails are locally strongly extended (in the framework of the SF model, the maximal stretching of unstructured protein corresponds to 1 aa residue per unit distance a). Outside of the proximal region the extension of the M tail decreases, and the external part of the tail adopts a coil conformation (manifested by the peripheral peak in the polymer density profile $\varphi_M(z)$). Such conformation of a projection domain resembles a flower: a strongly and uniformly stretched segment (stem) is crowned by a coil-like terminal domain. In neutral polymeric systems, flowerlike conformation was predicted for a long chain admixed in a polymer brush of shorter ones (26,27). Here, the expulsion of the long chain outside of the brush of short chains was caused by repulsive short-range monomer-monomer interactions. In a charged neurofilament brush the shortest (L) tails give rise to the electric field that expels the ionized M projection domains from

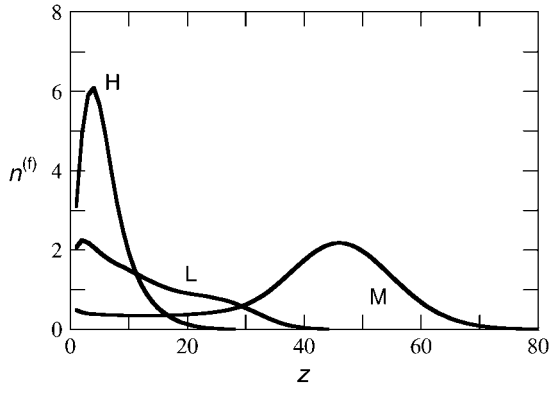

FIGURE 6 The number of monomers $n(z)$ per unit length a ($a = 6$ Å) of the NF counter as a function of the distance z from the backbone. As in Fig. 3, the pH = 7 and the ionic strength $c_s = 1 \times 10^{-2}$ M.

the proximal region of the NF brush and orients the stem of the M tail normally to the backbone. The analysis of the volume fraction profile $\varphi_L(z) \sim (R/a+z)^{-\beta_L}$ indicates that the shortest L tails are extended with respect to their Gaussian size $R_{G,L} = a\sqrt{N_L}$ (the thickness of the proximal L-region of the NF brush, $\Delta_L \simeq 30a > R_{G,L} \approx 12a$), and the exponent β_L is close to 2. Fig. 6 demonstrates that $n_L(z)$ is a decreasing function of z. However, in contrast to the distribution of end monomers for the M tails (almost no free ends of any M tails are found in the proximal region, Fig. 4), the distribution of end monomers for the L tails is rather wide. As a result, the apparent hyperstrong stretching of the L-chains ($\beta_L > 1$) is relaxed. The distribution of the polymer density $\varphi_H(z)$ is not approximated by a power law dependence in any region of the NF brush. This indicates rather that the longest tails envelop the backbone of the neurofilament (the H tails are confined in a cylindrical layer with thickness Δ_H of ~10–15a). Note the Gaussian size of the H tail, $R_G = a\sqrt{N_H} \approx 23a > \Delta_H$. Our preliminary data (not shown) indicates that the cleavage of both M and L tails does not significantly alter the density profile of the H tails. This implies that the conformation of the H tail is mostly determined by the electrostatic and hydrophobic interactions within H projection domains. Switching off hydrophobic attraction (Fig. 3, *c* and *d*) leads to a noticeable increase in the size of the H tails ($\Delta_H \simeq 30 - 35a$), pointing, thereby, to the possible predominance of nonelectrostatic interactions. The analysis of the NF brush reorganization, upon a variation of the ionic strength, may elucidate the respective roles of the electrostatic and hydrophobic contributions in the H-tail conformation. More details about the equilibrium conformation of the H tails can be obtained by using the two-dimensional SF model that allows for polymer density gradients in both the z-direction and the longitudinal direction along the NF backbone. We will report on these issues in a future publication.

5. Fig. 3, *a* and *b*, demonstrates that in a dephosphorylated NF the cutoff for the volume fraction profile of the M tails (corresponding to the external boundary of a NF brush) is found at $z \approx 65$ or, equivalently, $za \approx 38$ nm. As we demonstrate below, the phosphorylation of all KSP repeats in the H and M tails shifts the external boundary of the NF brush to $\sim z \approx 80$ ($za \approx 48$ nm). These values are consistent with experimental findings from atomic force microscopy on the range of the repulsive force from the individual filament backbone (28–31) and the interfilament distances in the axon in mouse sciatic nerve (6). They are also consistent with the interfilament spacing in axons of the peripheral nervous system (32). We emphasize that no adjustable parameters were used in the SCF calculation, and the values for a monomer size a = 5–6 Å and for the Flory interaction parameter χ = 0–2 are typical for flexible polymers in different solvents (19,25).
6. According to our SCF modeling, the NF polymer brush is a rather dilute system. The maximal value of polymer volume fraction is ~0.1 (or equivalently the volume filling of 10%) that is found near the backbone of the neurofilament. Much smaller values for the polymer volume fraction are found in the proximal (intermediate) region and the peripheral part of the brush. A lot of space inside the neurofilament brush suggests that transport and enzymatic axonal processes are sterically unhindered by the presence of the side arms. The low average content of aa residues inside the NF brush can hardly block the approach of ATP molecules and enzymes to the H tails enveloping the backbone of the neurofilament. At this stage it is of interest to mention that the distributions of the C-segments, that is, the serines within the KSP repeats of the H-chain and of the M-chain, are well separated. As shown in Fig. 7 these serines of the H-chain are very close to the backbone, whereas those of the M chain are in the coil region, i.e., near the brush periphery. The schematic representation of a dephosphorylated NF brush, which accumulates schematically our findings, is presented in Fig. 8 *a*.

Effect of phosphorylation

We now briefly consider what happens to the equilibrium internal structure of the NF brush upon the phosphorylation of the H and M tails. A more detailed analysis will be presented in a separate report. As mentioned in the introduction, we consider here moderate levels of phosphorylation that involve only KSP repeats in the H and M tails. Although each transfer of a phosphate from ATP changes the charge of the KSP repeat from +1 to −1, we smear the total acquired charge ΔQ_H and ΔQ_M among all KSP repeats within the H and M tails. In other words, we introduce an effective valence v_c of a serine in a KSP repeat which changes from 0 to −2 upon the uptake of the negative charge

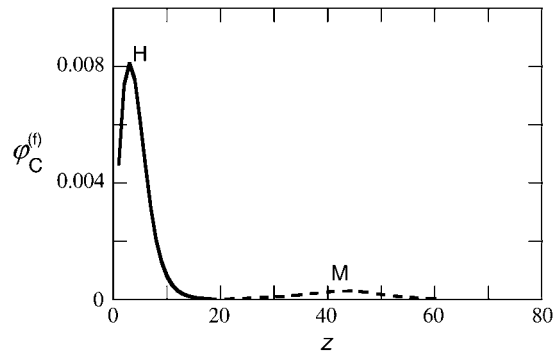

FIGURE 7 The volume fraction profile of the C-segments of the H-chain (*solid line*) and the M-chain (*dashed line*). Parameters as in Fig. 3, *a* and *b*.

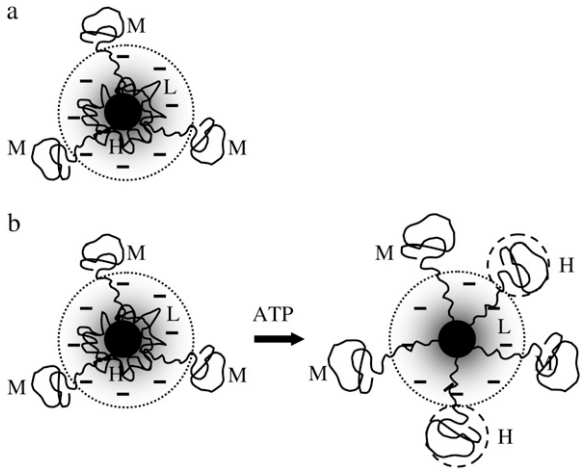

FIGURE 8 A schematic illustration of the equilibrium brush structure in a dephosphorylated NF (*a*), and the transformation of the NF brush upon phosphorylation (*b*). The dotted circle outlines the negatively charged proximal region of side arms L. The dashed circle outlines the KEP domain of side-arm H expelled from the NF backbone due to the phosphorylation.

due to phosphorylation. The total charge ΔQ acquired by a tail is then expressed as $\Delta Q = v_c N_{KSP}$ where N_{KSP} is the total number of KSP repeats in the tail. (The value of $v_c = -1$ corresponds to the state with 1/2 of all KSP repeats phosphorylated.)

Fig. 9 quantifies how the polymer volume fraction profiles for the H, M, and L tails change progressively upon the uptake of negative charge ΔQ by the KSP repeats (here and below ΔQ is normalized by the elementary charge e). All plots correspond to model f that accounts for the specific positioning of the KSP repeats in both the H and M tails. Fig. 9 *a* coincides with the result of Fig. 3 *a* for a dephosphorylated NF with $\Delta Q = 0$ and is replotted here for convenience. The details of this case have been discussed above. Fig. 9, *b–d*, corresponds to the subsequent increase in the negative charge $\Delta Q_H = -20$, $\Delta Q_H = -40$, and $\Delta Q_H = -80$, respectively. (Subscript H indicates the amount of charge acquired by the longest tail H.)

Fig. 9 indicates that the initial uptake of negative charge does not cause any significant changes in polymer distribution (Fig. 9 *b*). When almost half of all KSP repeats are phosphorylated, $\Delta Q_H = -40$, $v_c \approx -1$ (Fig. 9 *c*), the volume fraction profile of the H tails changes dramatically. The long tails exhibit a noticeable disproportionation: part of the H tails still envelops the backbone of the NF, whereas the remainder of the H tails are expelled to the outside, approaching the strongly extended M tails. A further uptake of negative charge (Fig. 9 *d*) demonstrates that all H tails left the backbone zone and acquired conformations reminiscent of the M tail. Due to the uptake of negative charges by the M tails, the NF brush expands, and the external boundary is shifted to $z = 80$ (the brush thickness increases by $\sim$10 nm with respect to the dephosphorylated NF).

The analysis of the decay of the polymer volume fractions of the H tails, $\varphi_H(z)$, indicates that the conformations of the M and H tails are now almost similar. Both are strongly and almost uniformly stretched in the proximal region of the brush and become coiled at the brush periphery. Fig. 8 *b* illustrates schematically the transformation of the NF brush structure upon phosphorylation.

A remarkable conformational transition in the H projection domain due to the NF phosphorylation (expulsion of the terminal KEP segment of the H tail to the periphery of the NF

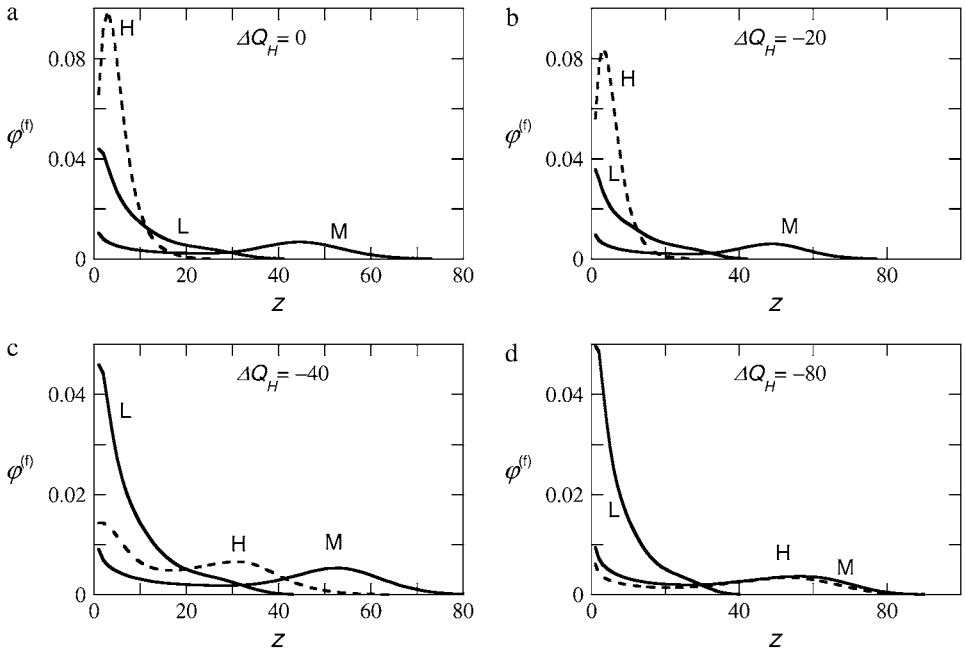

FIGURE 9 How the volume fraction distributions change upon phosphorylation of the KSP repeats for the H (*dashed*), M, and L tails in the fine model *f*. The value of the charge $\Delta Q_H \equiv \Delta Q_H/e$ indicated in the graphs increases going from graph *a* to *d*. The profiles of the H-chain are dashed, the others are represented by solid lines.

brush) enhances the availability of terminal domains for complexation. Indeed, in a dephosphorylated NF ($v_c = 0$) virtually all terminal KEP domains are localized near the NF core. To form a cross bridge between two dephosphorylated NFs, each of the two KEP domains, must be first relocated from the preferred position near the NF core to the NF brush periphery. The free energy penalty for this process is $\delta G > 0$. The phosphorylation of KSP repeats in the central part of the H tail perturbs the terminal KEP domain weakly, and it is reasonable to assume that the free energy of complexation between two KEP domains $\Delta G_{\text{complex}} < 0$ is almost independent of the level of NF phosphorylation (value of v_c). The total free energy change due to cross-bridging is $\Delta G = \Delta G_{\text{complex}} + \delta G > \Delta G_{\text{complex}}$. In contrast, in a phosphorylated NF (with $v_c \lesssim -2$) the terminal KEP domains are already localized at the periphery of the NF brush, thus yielding $\delta G = 0$, and $\Delta G \approx \Delta G_{\text{complex}}$. Therefore, the phosphorylation of the NF projection domains decreases ΔG and, thereby, promotes the formation of cross bridges between neurofilaments. In the axonal network the electrostatic interactions between NFs are weak (the Debye screening length is much smaller than the thickness of the NF brush). The relative sizes of the KEP domain and the remainder of the H tail suggest that cross-bridging will not strongly affect the thickness of the NF brush. Therefore, the phosphorylation-induced increase in the propensity of H tails to cross-bridging is also expected in axonal NF network. The specific details following from a detailed SCF modeling will be reported separately.

CONCLUSIONS

The self-consistent field SF method was applied to investigate the equilibrium structure of the human neurofilament brush. The modeling was performed with both a simple and a more refined coarse-graining of the actual aa sequences of the projection domains of the NF proteins. Both models revealed an inhomogeneous structure of the NF brush with a clear predominance of the electrostatic interactions. Different solubilities of various aa residues in water were accounted for in the refined model *f*, which predicts a higher density of aa residues near the backbone of the NF. Our study demonstrated a few distinct novel features in the NF brush organization.

Previous studies and reviews on NF subunit proteins emphasized the role of NF-L protein as an important partner in L-M and L-H heterodimer association (3,4) and in other regulatory processes in neuronal cells (1,33,34). The results of our SCF modeling demonstrate that the projection domains of the NF-L protein also play a distinct role in mediating the internal structure of the NF brush. Strongly charged L tails create a potential well (zone with a negative electrostatic potential around the backbone of the NF). In a dephosphorylated neurofilament, the long polyampholytic H tails are totally embedded into this zone, whereas the negatively charged intermediate M tails are expelled to the periphery of the brush. The flowerlike conformation of the M tail is a direct consequence of the electrostatic field created by the brush of the short L tails.

The ionization of the KSP repeats in the NF-H and NF-M proteins leads to an increase in the NF brush size (and, thereby, the interfilament distance) and triggers a major relocation of the H tails from the backbone of the NF to the periphery of the brush. This transition takes place when almost half of the KSP repeats in the H and M tails are phosphorylated. Moreover, the H projection domain adopts a flowerlike conformation upon further phosphorylation of the neurofilament. Similarly to the M tail, the H tail becomes strongly stretched near the backbone due to the brush of the L tails. The phosphorylation of the KSP repeats in the central part of the H tail does not perturb its terminal cross-bridging (KEP) domain, which moves to the periphery of the NF brush and becomes more available for complexation. The SCF modeling therefore predicts that the phosphorylation of the NFs in neurites may lead to two simultaneous effects: the increase in the interfilament distance (and, thereby, in the caliber of large axons) and the stabilization of cross bridges that keep the neurofilament network intact.

Our current study focuses on the equilibrium structure of an individual NF under the conditions of physiological pH $\sim$ 7 and relatively low ionic strength (0.01 M of 1:1 salt). Clearly, the intraaxonal pH and salinity may vary, particularly in pathological conditions. Exploring the NF brush structure in changing environmental conditions (pH, salinity, presence of multivalent ions, etc.) may elucidate how these factors affect the structure of the neurofilament cytoskeleton in vivo. In our forthcoming article we will report how the pH and the solution salinity affect the reorganization of the NF brush upon enzymatic phosphorylation of the projection domains.

The authors acknowledge financial support from Dutch National Science Foundation and Russian Foundation for Basic Research through joint project No. 047-017-026 ''Polymers in Nanomedicine: Design, Synthesis and Study of Inter-Polymer and Polymer-Virus Complexes in Search of Novel Pharmaceutical Strategies''. E.B.Z. acknowledges partial support from the Russian Foundation for Basic Research (RFBR grant No. 05-03-33126).

REFERENCES

1. Julien, J. P. 1999. Neurofilament functions in health and disease. *Curr. Opin. Neurobiol.* 9:554–560.
2. Hoffman, P. N., D. W. Cleveland, J. W. Griffin, P. W. Landers, N. J. Cowan, and D. L. Price. 1987. Neurofilament gene expression: a major determinant of axonal caliber. *Proc. Natl. Acad. Sci. USA.* 84:3472–3476.
3. Janmey, P. A., J.-F. Leterrier, and H. Herrmann. 2003. Assembly and structure of neurofilaments. *Curr. Opin. Colloid Interface Sci.* 8:40–47.
4. Hisanaga, S.-I., and N. Hirokawa. 1990. Molecular architecture of the neurofilament. II. Reassembly process of neurofilament L protein in vitro. *J. Mol. Biol.* 211:871–882.

5. Liu, L., X. Tong, S. Pang, and Z. Zhai. 1999. The periodicity in the structure of native neurofilaments studied with scanning tunneling microscopy. *Appl. Surf. Sci.* 144–145:644–647.

6. Kumar, S., X. H. Yin, B. D. Trapp, J. H. Hoh, and M. E. Paulatis. 2002. Relating interactions between neurofilaments to the structure of axonal neurofilament distribution through polymer brush models. *Biophys. J.* 82:2360–2372.

7. Hirokawa, N. 1982. Cross-linker system between neurofilaments, microtubules and membranous organelles in frog axons revealed by the quick-freeze, deep-etching method. *J. Cell Biol.* 94:129–142.

8. Rao, M. V., M. K. Houseweart, T. L. Williamson, T. O. Crawford, J. Folmer, and D. W. Cleveland. 1998. Neurofilament-dependent radial growth of motor axons and axonal organization of neurofilaments does not require the neurofilament heavy subunit (NF-H) or its phosphorylation. *J. Cell Biol.* 143:171–181.

9. Elder, G. A., V. L. Friedrich, Jr., C. Kang, P. Bosco, A. Gourov, P. H. Tu, B. Zhang, V. M. Lee, and R. A. Lazzarini. 1998. Requirement of heavy neurofilament subunit in the development of axons with large calibers. *J. Cell Biol.* 143:195–205.

10. Jacomy, H., Q. Zhu, S. Couillard-Despres, M. Beaulieu, and J. P. Julien. 1999. Disruption of type IV intermediate filament network in mice lacking the neurofilament medium and heavy subunits. *J. Neurochem.* 73:972–984.

11. Zhu, O., M. Lindenbaum, F. Levavasseur, H. Jacomy, and J. P. Julien. 1998. Disruption of the NF-H gene increases axonal microtubule content and velocity of neurofilament transport: relief of axonopathy resulting from the toxin β, β'-iminodipropionitrile. *J. Cell Biol.* 143:183–193.

12. Ma, D. M., L. Descarries, K. D. Micheva, Y. Lepage, J. P. Julien, and G. Doucet. 1999. Severe neuronal losses with age in the parietal cortex and ventrobasal thalamus of mice transgenic for the human NF-L neurofilament protein. *J. Comp. Neurol.* 406:433–448.

13. Mukhopadhyay, R., S. Kumar, and J. H. Hoh. 2004. Molecular mechanisms for organizing the neuronal cytoskeleton. *Bioessays.* 26:1–9.

14. Napper, D. H. 1983. Polymeric Stabilization of Colloid Dispersions. Academic Press, London.

15. Zhulina, E. B., O. V. Borisov, and V. A. Priamitsyn. 1990. Theory of steric stabilization of colloid dispersions by grafted polymers. *J. Colloid Interface Sci.* 137:495–511.

16. Balazs, A. C., C. Singh, and E. B. Zhulina. 1998. Stabilizing properties of copolymers adsorbed on heterogeneous surfaces: a model for the interactions between a polymer-coated influenza virus and a cell. *Macromolecules.* 31:6369–6379.

17. De Kruif, C. G., and E. B. Zhulina. 1996. Kappa-casein as a polyelectrolyte brush on the surface of casein micelles. *Colloids Surf. A.* 117:151–159.

18. Turnier, R., and C. G. de Kruif. 2005. Stability of casein micelles in milk. *J. Chem. Phys.* 117:1290–1295.

19. Fleer, G. J., M. A. Cohen-Stuart, J. M. H. M. Scheutjens, T. Cosgrove, and B. Vincent. 1993. Polymers at Interfaces. Chapman & Hill, London.

20. Leermakers, F. A. M., P. J. Atkinson, E. Dickinson, and D. S. Horne. 1996. Self-consistent field modeling of adsorbed β-casein: effects of pH and ionic strength on surface coverage and density profile. *J. Colloid Interface Sci.* 178:681–693.

21. Van den Oever, J. M. P., F. A. M. Leermakers, G. J. Fleer, V. A. Ivanov, N. P. Shusharina, A. R. Khokhlov, and P. G. Khalatur. 2002. Coil-globule transition for regular, random and specially designed copolymers: Monte Carlo simulation and self-consistent field theory. *Phys. Rev. E.* 65:041708-1/13.

22. Claessens, M. M. A. E., B. F. van Oort, F. A. M. Leermakers, F. A. Hoekstra, and M. A. Cohen Stuart. 2004. Charged lipid vesicles: effects of salts on bending rigidity, stability, and size. *Biophys. J.* 87:3882–3893.

23. Kik, R. A., F. A. M. Leermakers, and J. M. Kleijn. 2005. Molecular modeling of lipid bilayers and the effect of protein-like inclusions. *Phys. Chem. Chem. Phys.* 7:1996–2005.

24. Israëls, R., F. A. M. Leermakers, and G. J. Fleer. 1994. On the theory of grafted weak polyacids. *Macromolecules.* 27:3087–3093.

25. Zhulina, E. B., A. Adam, S. Sheiko, I. LaRue, and M. Rubinstein. 2005. Diblock copolymer micelles in a dilute solution. *Macromolecules.* 38:5330–5351.

26. Skvortsov, A. M., L. I. Klushin, and A. A. Gorbunov. 1997. Long and short chains in a polymeric brush: a conformational transition. *Macromolecules.* 30:1818.

27. Skvortsov, A. M., L. I. Klushin, and F. A. M. Leermakers. 2002. Exactly solved polymers models with conformational escape transitions of a coil-to-flower type. *Europhys. Lett.* 58:292–298.

28. Brown, H. G., and J. H. Hoh. 1977. Entropic exclusion of neurofilament side arms: a mechanism for maintaining interfilament spacing. *Biochemistry.* 36:15035–15040.

29. Hoh, J. H. 1998. Functional protein domains from the thermally driven motion of polypeptide chains: a proposal. *Proteins Struct. Funct. Genet.* 32:223–228.

30. Mukhopadhyay, R., and J. H. Hoh. 2001. AFM force measurements on microtubule-associated proteins: the projection domain exerts a long-range repulsive force. *FEBS Lett.* 505:374–378.

31. Kumar, S., and J. H. Hoh. 2004. Modulation of repulsive forces between neurofilaments by sidearm phosphorylation. *Biochem. Biophys. Res. Comm.* 324:489–496.

32. Hsieh, S. T., T. O. Crawford, and J. W. Griffin. 1994. Neurofilament distribution and organization in the myelinated axons of the peripheral nervous system. *Brain Res.* 642:316–326.

33. Crow, J. P., Y.-Z. Ye, M. Strong, M. Kirk, S. Barnes, and J. S. Beckman. 1997. Superoxide dismutase catalyzes nitration of tyrosines by peroxynitrite in the rod and head domains of neurofilament-L. *J. Neurochem.* 69:1945–1953.

34. Chen, J. G., T. Nakata, Z. Z. Zhang, and N. Hirokawa. 2000. The C-terminal tail domain of neurofilament protein H (NF-H) forms the cross bridges and regulates neurofilament bundle formation. *J. Cell Sci.* 113:3861–3869.